THE JOURNAL OF BIOLOGICAL CHEMISTRY VOL. 289, NO. 40, pp. 27992–28005, October 3, 2014

Molecular Characterization of Arylsulfatase G

*EXPRESSION, PROCESSING, GLYCOSYLATION, TRANSPORT, AND ACTIVITY**

Received for publication, May 23, 2014, and in revised form, August 7, 2014 Published, JBC Papers in Press, August 18, 2014, DOI 10.1074/jbc.M114.584144

Björn Kowalewski[‡], Torben Lübke[‡], Katrin Kollmann[§], Thomas Braulke[§], Thomas Reinheckel[¶], Thomas Dierks[‡1], and Markus Damme[‡2]

From the [‡]Department of Chemistry, Biochemistry I, Bielefeld University, 33615 Bielefeld, the [§]Department of Biochemistry, Children's Hospital, University Medical Center Hamburg-Eppendorf, Hamburg 20246, and the [¶]Institute of Molecular Medicine and Cell Research and BIOSS Centre for Biological Signalling Studies, University of Freiburg, Freiburg 79104, Germany

Background: Lysosomal arylsulfatase G (ARSG) is critical in heparan sulfate degradation.
Results: ARSG is differentially expressed, processed, and transported in tissues involving a membrane-associated pre-lysosomal precursor; processing is dispensable for enzymatic activity.
Conclusion: Although its lysosomal function is established, ARSG maturation and lysosomal targeting involve nontypical steps.
Significance: These characteristics of ARSG need consideration when screening for ARSG-deficient mucopolysaccharidosis patients.

Arylsulfatase G (ARSG) is a recently identified lysosomal sulfatase that was shown to be responsible for the degradation of 3-*O*-sulfated *N*-sulfoglucosamine residues of heparan sulfate glycosaminoglycans. Deficiency of ARSG leads to a new type of mucopolysaccharidosis, as described in a mouse model. Here, we provide a detailed molecular characterization of the endogenous murine enzyme. ARSG is expressed and proteolytically processed in a tissue-specific manner. The 63-kDa single-chain precursor protein localizes to pre-lysosomal compartments and tightly associates with organelle membranes, most likely the endoplasmic reticulum. In contrast, proteolytically processed ARSG fragments of 34-, 18-, and 10-kDa were found in lysosomal fractions and lost their membrane association. The processing sites and a disulfide bridge between the 18- and 10-kDa chains could be roughly mapped. Proteases participating in the processing were identified as cathepsins B and L. Proteolytic processing is dispensable for hydrolytic sulfatase activity *in vitro*. Lysosomal transport of ARSG in the liver is independent of mannose 6-phosphate, sortilin, and Limp2. However, mutation of glycosylation site N-497 abrogates transport of ARSG to lysosomes in human fibrosarcoma cells, due to impaired mannose 6-phosphate modification.

Sulfatases are a group of enzymes that catalyze the hydrolysis of sulfate esters from different types of substrate molecules, including sulfolipids and sulfated glycosaminoglycans (GAGs).[3] By means of bioinformatics, 17 and 14 sulfatases have been identified in the human and murine genome, respectively, of which 13 have been characterized biochemically (1–3). Eight of these sulfatases are localized in lysosomes, where at least six of them are involved in the degradation of the GAGs heparan sulfate, dermatan sulfate, chondroitin sulfate, and keratan sulfate (4). The natural substrate of the very recently described lysosomal arylsulfatase K is yet unknown (2). Arylsulfatase A catalyzes the desulfation of the sulfolipid cerebroside 3-sulfate (5). Deficiencies of each of the GAG-degrading lysosomal sulfatases lead to mucopolysaccharidoses (MPS) characterized by an accumulation of sulfated GAG chains in lysosomes. Affected patients often show neurological symptoms and systemic organ defects leading to premature death (6).

One of the recently characterized sulfatases is arylsulfatase G (ARSG). In overexpressing cells, His-tagged human ARSG is detected as a 63-kDa glycoprotein that binds to mannose 6-phosphate receptors (MPR) and co-localizes with LysoTracker, thereby classifying it as a lysosomal protein. *ARSG* mRNA is broadly expressed in different tissues. The recombinant protein is enzymatically active against the arylsulfate pseudosubstrate *p*-nitrocatechol sulfate (pNCS) under acidic conditions (3).

We have previously reported on the generation of *Arsg* knock-out (KO) mice (7) developing a lysosomal storage disease phenotype with accumulation of enlarged and mostly electron-lucent vacuoles, resembling those of other mouse models for mucopolysaccharidoses but with an attenuated phenotype. Increased amounts of GAGs were detected in various tissues. Examination of the GAG storage material derived from these KO mice identified it as heparan sulfate, and further detailed analysis of the nonreducing end revealed 3-*O*-sulfated *N*-sulfoglucosamine (GlcNS3S) as the natural substrate of ARSG. We therefore classified this new lysosomal storage disease as MPS IIIE, consistent with its function in the lysosomal degradative pathway of glucosamine residues in heparan sulfate. Recently,

* This work was supported by Deutsche Forschungsgemeinschaft Grant DI 575/6 (to T. D.).
[1] To whom correspondence may be addressed: Dept. of Chemistry, Biochemistry I, Bielefeld University, 33615 Bielefeld, Germany. Tel.: 521-106-6918; Fax: 521-106-6014; E-mail: thomas.dierks@uni-bielefeld.de.
[2] To whom correspondence may be addressed: Institut für Biochemie, Christian-Albrechts-Universität zu Kiel, 24098 Kiel, Germany. Tel.: 431-880-2218; Fax: 431-880-2238; E-mail: mdamme@biochem.uni-kiel.de.
[3] The abbreviations used are: GAG, glycosaminoglycan; Man-6-P, mannose 6-phosphate; PNS, postnuclear supernatant; P, pellet; S, soluble; IP, immunoprecipitation; ER, endoplasmic reticulum; MPR, mannose 6-phosphate receptor; GlcNS3S, 3-*O*-sulfated *N*-sulfo-glucosamine; pNCS, 4-nitrocatechol sulfate; PNGaseF, peptide-*N*-glycosidase F; EndoH, endoglycosidase H; MEF, mouse embryonic fibroblast; DNJ, 1-deoxynojirmycin; ML, mitochondria/lysosomal; Pdi, protein-disulfide isomerase; ki, knock-in.

mutations in *ARSG* have been described in dogs with a lysosomal storage phenotype mostly affecting the nervous system and similarities to neuronal ceroid lipofuscinosis (8).

Although the natural substrate of ARSG is known and its role in the degradation of heparan sulfate was unequivocally shown by our KO approach, no data are available on biochemical properties of the endogenous enzyme, including its expression in tissues, post-translational modifications, or mode of transport to lysosomes. In this study, we report on in-depth analysis of tissue expression, proteolytic processing, and nontypical lysosomal transport mechanisms of ARSG.

EXPERIMENTAL PROCEDURES

Mice—ARSG-deficient mice were described previously (7). Mice deficient for the lysosomal transport receptors (Limp2 and sortilin) or GlcNAc-1-phosphotransferase knock-in (coded by *Gnptab*) mice were described previously (9–11). Protease-deficient mice were described as follows: cathepsin B KO (12); cathepsin H KO (13); cathepsin L KO (14); asparagine endopeptidase KO (15); and cathepsin D KO (16). All animal experiments were approved by local authorities. Mice were kept on a 12-h light and 12-h dark schedule with *ad libitum* access to food and water.

Antibodies and Chemicals—The following commercial antibodies were used throughout the study: ARSG (R&D Systems), raised against full-length recombinant murine ARSG protein (Gly-17–Val-525) derived from Chinese hamster ovary cells; Gapdh (Santa Cruz Biotechnology); actin (Sigma); RGS-His (Qiagen); protein-disulfide isomerase (Pdi) (Cell Signaling). Monoclonal antibody against Lamp1 (clone 1D4B) was obtained from Developmental Studies Hybridoma Bank and maintained at the University of Iowa, Department of Biology, Iowa City, IA 52242. Antisera and monoclonal antibodies raised against cathepsin D (17), Rab5a (18), and Npc2 (19) were described previously. If not stated otherwise, chemicals were purchased from Sigma.

Transfection and Cell Culture—HT1080 human fibrosarcoma cells (ATCC CCL-121) were used to generate stably expressing cell lines. Mouse embryonic fibroblasts (MEF) were prepared from aforementioned mouse strains and immortalized by either autoimmortalization or transfection with the SV40 large T antigen in the pMSSVLT vector (20). Transfection was carried out using the Lipofectamine LTX transfection kit (Invitrogen) according to manufacturer's recommendation. Stably transfected cells were selected with hygromycin B (PAA Laboratories).

Construction of Expression Plasmids—The murine *Arsg* cDNA was generated from wild type mouse kidney mRNA using the Omniscript RT-PCR kit (Qiagen) with the primer GAAGTAAACCCACCTGTCTACAG. Single-stranded cDNA was amplified by PCR using Pfu II Ultra DNA polymerase and the primers CGGGAGTCTTCGTGTCTTAC and GAAGTAAACCCACCTGTCTACAG. Restrictions sites for EcoRV, NotI, and a sequence coding for C-terminal RGS-His_6 tag followed by a stop codon were added by nested PCR with the primers TACGATATCATGGGCTGGCTCTTTCTAAAG and TACGCGGCCGCTTATCCGTGATGGTGATGGTGATGCGATCCTCTTCCGACCGGTTGGCAACGGCAGGTAG (restriction sites underlined). The PCR product was digested with EcoRV and NotI (New England Biolabs) and directly cloned into the pcDNA3.1(+) Hygro vector (Invitrogen). Mutations in the murine *Arsg* cDNA were introduced using the QuikChange mutagenesis protocol (Stratagene) with the following primer: N117Q, GGGGGGCTTCCAGTC**CAG**GAGACCACCTTGGC; N215Q, CGTGGAGCAGCCTGTG**CAG**CTGAGCGGCCTTGCAC; N356Q, CTGGCAGAGTTCCAGCC**CAG**GTCACTAGCACCGCC; N497Q, CAAGACATCGCTGATGAC**CAG**AGCTCCCGAGCAGAC (mutated triplet in bold). The coding region of all constructs was sequenced. The pCI-neo vector containing the human ARSG-RGS-His_6 construct was described previously (5).

Tissue and Cell Extracts—Both homogenates and lysates were prepared in ice-cold lysis buffer (TBS with 1 mM phenylmethylsulfonyl fluoride (PMSF), 5 mM iodoacetamide, 1 mM EDTA and either 0.5% (v/v) (homogenates) or 0.1% (v/v) Triton X-100 (cell lysates)). Tissues were homogenized using a Potter-Elvehjem homogenizer with three strokes and subsequent sonification (three times for 20 s, 40% intensity, Branson Sonifier). Homogenates were cleared by centrifugation at 18,000 × *g* at 4 °C for 15 min. Cell lysates were prepared by sonification and spinning. Protein concentration was determined using DC assay (Bio-Rad) with bovine serum albumin as standard.

Immunoblotting—SDS-PAGE and immunoblot analysis was performed by standard procedures using polyvinylidene difluoride (PVDF) membrane. In the case of nonreducing SDS-PAGE, cell lysates were treated with PBS containing 50 mM *N*-ethylmaleimide prior to harvesting to avoid disulfide shuffling.

Activity Assays—Sulfatase activity on immunoprecipitates after ARSG IP was measured using the pseudosubstrate pNCS at a concentration of 10 mM in 500 mM sodium acetate buffer, pH 5.6. The reaction was terminated by addition of 1 M NaOH. Absorbance was measured with microplate M200 reader (Tecan) at 515 nm.

Glycosidase Treatment—Cell homogenates were denatured in 0.33% SDS and 167 mM 2-mercaptoethanol at 95 °C for 5 min. After cooling, the samples were buffered with 111 mM Tris/HCl, 11 mM EDTA, pH 8.0 (for peptide *N*-glycosidase F (PNGaseF)), or 55.6 mM sodium acetate, pH 5.5 (for endoglycosidase H (EndoH)). Additionally, 1.1 mM PMSF and 1.1% CHAPS (PNGase F) or 0.11% CHAPS (EndoH) were added to the mixture. The glycoprotein was deglycosylated by adding 2 units of PNGase F or 5–10 milliunits of EndoH and subsequent incubation at 37 °C overnight.

Tritosome Preparation—Tritosomes were prepared as described previously (21). In brief, mice were injected with tyloxapol (Sigma) 4 days prior to sacrifice. The liver was removed and homogenized in a Potter-Elvehjem homogenizer with six strokes in iso-osmotic buffer containing 250 mM sucrose. Nuclei and debris were sedimented by centrifugation at 1,000 × *g* for 10 min. The postnuclear supernatant (PNS) was then centrifuged for 7 min at 56,000 × *g*. A pellet fraction containing mitochondria and lysosomes was obtained, washed in 250 mM sucrose, and resuspended in sucrose resulting in an ML fraction with a final density of ~1.21. The ML fraction (3.5 ml) was subjected to centrifugation on a discontinuous sucrose gra-

dient for 150 min at 110,000 × *g* (Sorvall TH-641) using sucrose solutions with densities of 1.15, 1.14, and 1.06, respectively. Lysosomes were collected at the interphase between ρ 1.14 and 1.06 sucrose.

Percoll Density Gradient Centrifugation—PNS was prepared by homogenization of the liver in a Potter-Elvehjem with six strokes in iso-osmotic buffer containing 250 mM sucrose and 3 mM imidazole, pH 7.4, followed by centrifugation for 10 min at 1,000 × *g*. The PNS was mixed with 90% Percoll™ in 250 mM sucrose, 3 mM imidazole, pH 7.4, to a final concentration of 50%. This mixture was centrifuged in a swing-out rotor at 30,000 × *g* for 90 min at 4 °C. Fractions were collected from top to bottom, and the Percoll™ was removed by centrifugation.

Metabolic Labeling—Cells were labeled with [^{35}S]methionine/cysteine (PerkinElmer Life Sciences), followed by immunoprecipitation with mARSG (600 ng) antibody, SDS-PAGE, and autoradiography as described for cathepsin D (22).

Membrane Association—Liver PNS was prepared as described for Percoll density centrifugation in 250 mM sucrose, 140 mM NaCl, and 10 mM Tris/HCl, pH 7.5. PNS was lysed by three rounds of thawing and freezing in ethanol cooled with dry ice followed by ultrasonification. The lysed PNS was then centrifuged for 30 min at 190,000 × *g* at 4 °C to separate membranes and soluble proteins. Membranes were washed once with homogenization buffer, and supernatants (containing soluble proteins) were pooled. Membranes were treated with 100 mM Na_2CO_3, pH 11, for 30 min on ice followed by centrifugation for 30 min at 190,000 × *g* at 4 °C (with membrane-associated proteins in the supernatant) (23). Integral membrane protein-containing fraction was resuspended in 0.5% Triton X-100 and centrifuged again, and the final pellet was dissolved in 2% SDS. 0.5 mM mannose 6-phosphate was included in buffers where indicated.

Inhibitor Experiments—MEFs were transfected with the *Arsg* cDNA, and 20 mM NH_4Cl was added to the growth medium 8 h after transfection. Cells were harvested 24 h after the medium change and processed as described above.

HT1080 cells were pretreated for 2 h with DNJ and after transfection were further incubated in the presence of either 5 or 20 mM DNJ for 48 h. After transfection, cells were harvested 48 h later and processed as described above.

Pulse-chase inhibitor experiments were carried out using transiently *mArsg*-transfected HT1080 cells, which were metabolically labeled with [^{35}S]methionine/cysteine. Medium was changed after 45 min to DMEM growth medium containing various protease inhibitors. Inhibitor concentrations were 1 mM 4-(2-aminoethyl)benzenesulfonyl fluoride, 40 μM E-64d, 100 μM pepstatin A, 100 μM leupeptin, 5 mM EDTA, 5 mM 1,10-phenanthroline, and a commercial protease inhibitor mixture according to the manufacturer's recommendations (Sigma). Cells were harvested after 8 h. Immunoprecipitation, SDS-PAGE, and autoradiography were carried out as described above.

Gel Filtration—Gel filtration was performed on a Superdex 200 HR 10/300 GL column (GE Healthcare) using the Ettan LC system (GE Healthcare). The soluble content of tritosomal fractions was applied to the column and eluted with 10 mM 2-(*N*-morpholino)ethanesulfonic acid, 150 mM NaCl buffer at a flow rate of 200 μl/min. Fractions of 250 μl were collected. Two standard runs with the molecular weight markers dextran blue, thyroglobulin, ferritin, β-amylase, alcohol dehydrogenase, albumin, ovalbumin, carbonic anhydrase, cytochrome *c*, and aprotinin were performed to calibrate the column and calculate a standard curve.

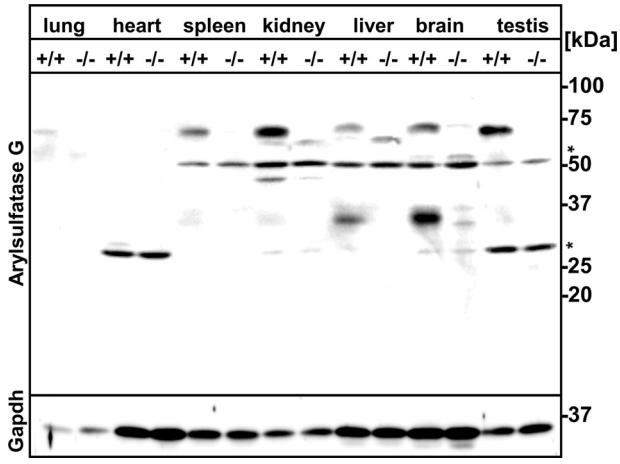

FIGURE 1. **ARSG is expressed and proteolytically processed in a tissue-dependent manner.** Tissue homogenates from $WT^{+/+}$ and *Arsg* $KO^{-/-}$ mice were analyzed by immunoblotting with an ARSG-specific antibody. A major specific band for ARSG at ~63-kDa can be detected at different levels in all tissues. An additional specific band is detected at ~34-kDa in the liver and notably in the brain, where most ARSG is proteolytically processed. Nonspecific bands are marked with *asterisks*. Gapdh immunoblots were used as loading control. Equal amounts of protein were loaded on the gels (120 μg/lane).

RESULTS

Tissue-specific Expression and Proteolytic Processing of ARSG—Mice deficient in ARSG exhibit lysosomal storage of heparan sulfate with terminal *N*-sulfoglucosamine-3-*O*-sulfate (GlcNS3S) residues at the nonreducing end. Storage pathology was demonstrated in liver, brain, and kidney (7). However, no data are available addressing the tissue distribution and biochemical characterization of endogenous ARSG at the protein level. To determine its expression, we evaluated commercially available antibodies for ARSG detection by immunoblot analyses (Fig. 1). Tissues from *Arsg* KO mice served as specificity controls. ARSG-specific bands of the expected molecular mass of 63 kDa for the glycosylated protein were detected in most tissues evaluated, including lung, spleen, kidney, liver, brain, and testis. None or only faint ARSG bands were detected in the heart and the lung, respectively. An additional strong immunoreactive band with a molecular mass of ~34 kDa was observed in the liver and even more abundant in brain lysates, where overall ARSG protein levels were highest among the evaluated tissues. These data show tissue-specific expression and proteolytic processing of the 63-kDa ARSG polypeptide.

Subcellular Distribution of the Processed and Unprocessed ARSG Forms—The lysosomal storage pathology of *Arsg* KO mice indicates a lysosomal localization, and ARSG was previously shown to co-localize with LysoTracker under overexpressing conditions (3). We evaluated the subcellular distribution of endogenous ARSG with particular attention to the different molecular forms. We therefore applied subcellular

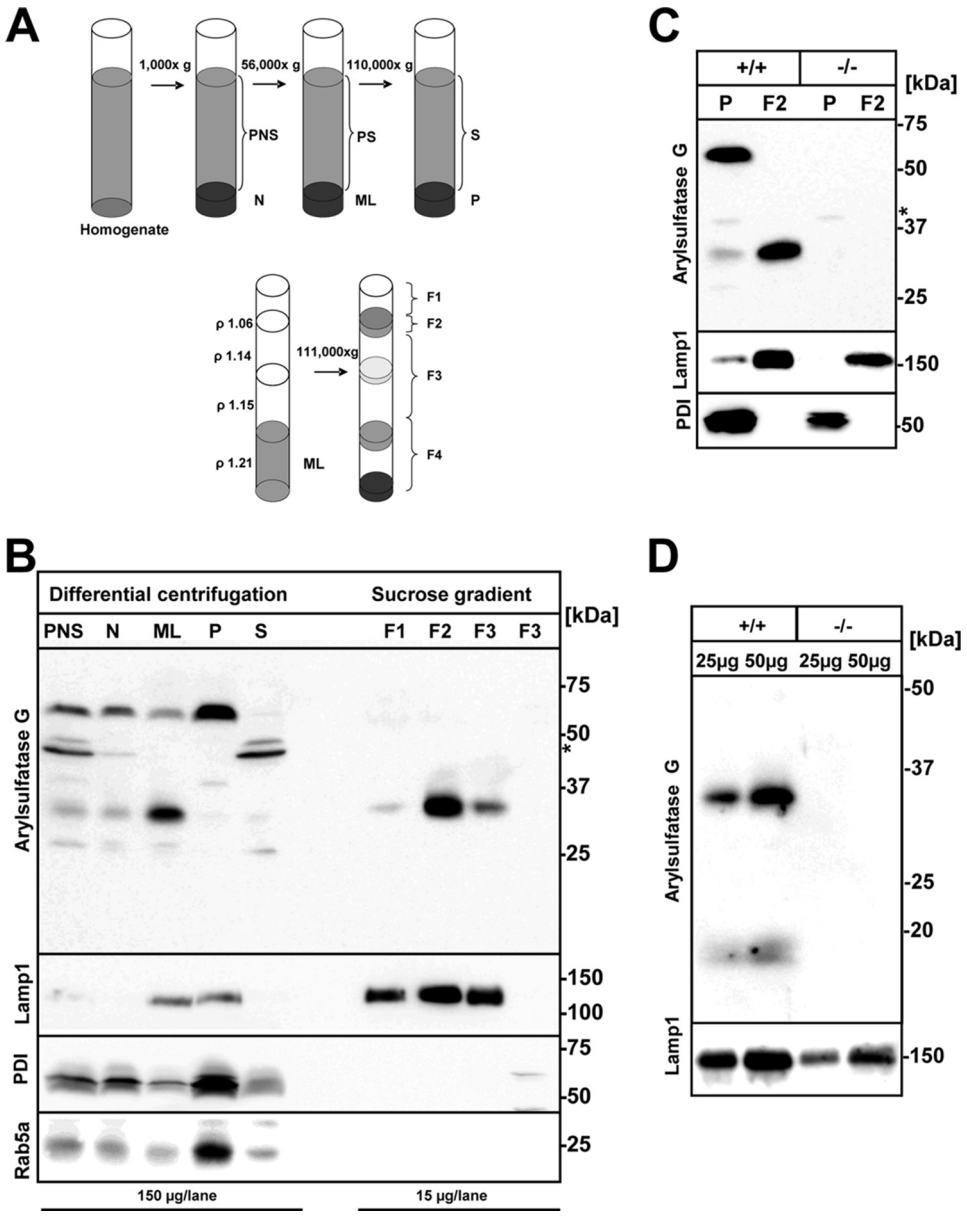

FIGURE 2. **Proteolytically processed fragments of endogenous ARSG localize to lysosomes, whereas the precursor localizes to microsomes.** *A,* subcellular fractionation scheme of liver homogenates from mice treated with tyloxapol. Postnuclear supernatants were differentially centrifuged, yielding a nuclear fraction and the supernatant (*PNS*) which was again centrifuged, yielding an ML fraction (light mitochondria, containing mitochondria and lysosomes) and a PS fraction, containing microsomes (*P*) and cytosol (*S*). The ML fraction was then loaded on a discontinuous sucrose gradient, leading to four fractions F1–F4 upon centrifugation. *B,* immunoblot analysis of all fractions showed the processed 34-kDa fragment enriched in the ML fraction. The 63-kDa precursor was significantly enriched in the microsomal fraction, which is essentially free of the 34-kDa fragment and contained Golgi apparatus, ER (see PDI as a marker) and early endosomes (see Rab5a as a marker). The 34-kDa form was further highly enriched in the F2 fraction, which contained highest amounts of lysosomal markers (Lamp1). Note differences in protein loading (PNS, N, ML, S, 150 μg; F1–F2,15 μg). *C,* loading of P and F2 fraction of WT and *Arsg*$^{-/-}$ mice verifies specific detection of both 63- and 34-kDa bands (P, 150 μg/lane; F2, 15 μg/lane). *D,* loading high amounts of the lysosomal fraction F2 revealed an additional processed band of ARSG at ~18-kDa.

fractionation of liver tissue using tyloxapol, a detergent causing a significantly reduced density of lysosomes allowing efficient purification ("tritosomes") (Fig. 2*A*) (24). Differential centrifugation of wild type mouse liver led to a nuclear fraction containing nuclei, nondisrupted cells and debris, and a PNS containing organelles and cytosol. Both the 63- and 34-kDa ARSG bands were found in PNS fraction as assessed by immunoblot analysis (Fig. 2*B*). Further separation of the PNS by centrifugation at 56,000 × *g* into an ML fraction and a PS fraction containing cytosolic components (S) and microsomes (P) revealed a strong enrichment of the 34-kDa band and a decreased amount of the 63-kDa band in the ML fraction, implicating lysosomal residence of the processed 34-kDa form. Further separation of P and S fractions by centrifugation at 110,000 × *g* quantitatively recovered the 63-kDa ARSG form in the microsomal fraction (P) but essentially no 34-kDa form. A nonspecific band of ~45 kDa was quantitatively separated and recovered in the cytosolic fraction (S). Enrichment of both early endosomes and endoplasmic reticulum (ER) in the microsomal P-fraction is shown by enrichment of the marker proteins Rab5a (early endosomes) and Pdi (ER), suggesting a pre-lysosomal/late endosomal localization of the 63-kDa form of ARSG (Fig. 2*B*).

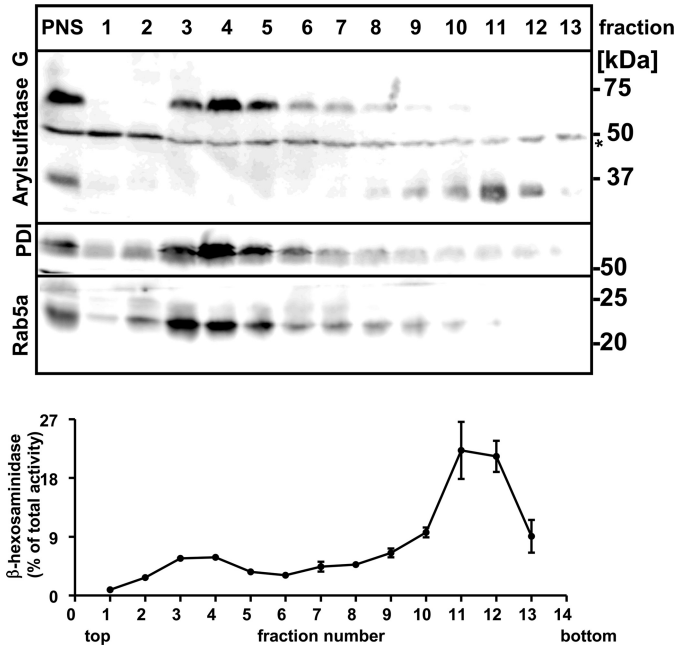

FIGURE 3. **ARSG precursor co-sediments with the endoplasmic reticulum.** PNS of liver homogenates ($n = 3$) were separated by centrifugation in 50% self-forming Percoll gradients. The 63-kDa precursor and the 34-kDa processed ARSG fragment were efficiently separated. The 34-kDa fragment was highly enriched in fractions with highest β-hexosaminidase activity (marker for lysosomes, see *bottom panel*), whereas the precursor co-sediments with Pdi (ER marker) rather than Rab5a, a marker for early endosomes (see *upper panels*).

The tyloxapol-loaded ML fraction was further separated by isopycnic centrifugation on a discontinuous sucrose density gradient. Thus, the majority of the processed ARSG form was recovered in the F2 fraction, which is enriched in lysosomal proteins as assessed by highest Lamp1 immunoreactivity (Fig. 2*B*). Of note, only 10% of total protein from fractions F1 to F4 was loaded compared with fractions derived from differential centrifugation, demonstrating 30–40-fold enrichment of the 34-kDa fragment in the F2 fraction, which is typically also observed for other lysosomal proteins in the tyloxapol-based fractionation experimental setup (21, 25).

Subcellular fractionation of liver derived from *Arsg* KO mice and subsequent immunoblot analysis confirmed specific detection of ARSG bands (Fig. 2*C*). Loading high amounts of lysosome-enriched F2 fractions (25 μg of protein) from wild type mice revealed an additional ARSG-specific band at ~18 kDa (Fig. 2*D*), indicating an even more complex processing pattern.

To prove the subcellular distribution of the different ARSG forms independent of the tyloxapol-induced lysosomal density shift used for tritosome preparation, we subjected liver PNS of untreated wild type mice to separation on a self-forming Percoll gradient (Fig. 3). Again, subcellular separation of the 63- and the 34-kDa band was validated. Although the majority of the 63-kDa precursor was found in fractions 3–5, the 34-kDa band was recovered in fractions 10–12 close to the bottom of the gradient, co-fractionating with the highest activity of the lysosomal marker enzyme β-hexosaminidase (Fig. 3, *bottom panel*). The distribution of lysosomal marker proteins is bimodal on density gradients due to localization in early endosomes of light density and late endosomal/lysosomal fractions (26, 27). To define fractions containing the pre-lysosomal 63-kDa precursor form of ARSG, we used marker proteins for the ER (Pdi) and early endosomes (Rab5a). Although fractions with the precursor ARSG contained both early endosome and ER markers, the distribution of ARSG closely resembled that of Pdi rather than that of Rab5a. We failed to detect ARSG at the endogenous level in MEFs by immunofluorescence, precluding any localization experiments by immunocytochemistry.

Membrane Association of the ARSG Precursor—As the ARSG sequence does not contain any obvious ER retention motif, we considered a membrane association of ARSG to cause ER residence, which we analyzed by carbonate extraction. PNS from liver was recovered as described before and lysed by four cycles of thaw-freezing followed by ultrasonication (Fig. 4*A*). Membranes were pelleted by centrifugation at 190,000 × *g*. As determined by immunoblot, the 63-kDa ARSG precursor was enriched in the membrane pellet (P), whereas in the soluble (S) fraction (containing soluble cytosolic and luminal proteins) almost exclusively the 34-kDa form was found (Fig. 4*B*). Cytosolic Gapdh, cathepsin D as a (partially) membrane-associated protein (28–30), and Lamp1 as an integral membrane protein served as loading controls. Approximately 60% of the entire ARSG pool was found in the membrane fraction. Treatment of the membrane fraction with 0.1 M Na_2CO_3 to dissociate membrane-associated proteins (23) followed by centrifugation released ~50% of the membrane-bound 63-kDa precursor from membranes and essentially all of the residual 34-kDa ARSG fragment. Surprisingly, however, still ~50% of the ARSG precursor was recovered in the membrane fraction, indicating tight binding to membranes. Membrane-bound cathepsin D was completely recovered in the supernatant upon Na_2CO_3 treatment, indicating that conditions for carbonate treatment were sufficient to release associated membrane proteins. Solubilization of the Na_2CO_3 pellet with 0.5% Triton X-100 was not sufficient to solubilize the entire residual pool of ARSG, and small amounts were solubilized only by SDS. Because the transport of most acid hydrolases to the lysosome is mediated by mannose 6-phosphate receptors, we determined whether the membrane association is mediated by binding to MPRs. However, including 5 mM mannose 6-phosphate (Man-6-P) into all buffers used for membrane extraction, to compete with binding to MPRs, did not affect membrane association, indicating that MPRs are not involved in the tight binding of ARSG to membranes.

To further determine the mode of interaction of the 63-kDa ARSG precursor with membranes, we applied different agents for membrane extraction like high salt buffer (1.5 M NaCl), 5 mM β-mercaptoethanol containing buffer or acidic sodium acetate buffer, pH 4.5 (Fig. 4*C*). However, only Triton X-100 efficiently, but not completely, released ARSG from membranes, and Na_2CO_3, as before, only partially solubilized the ARSG precursor. No effect was observed for NaCl, β-mercaptoethanol, or acidic buffer. Finally, we evaluated the membrane association of the lysosomal 34- and 18-kDa forms using tritosomal fractions (Fig. 4*D*). Neither the 34- nor the 18-kDa protein exhibited association with membranes.

Kinetics, Localization, and Products of Proteolytic ARSG Processing—Next we examined the kinetics of processing and the half-life of the intracellular ARSG forms by [^{35}S]methio-

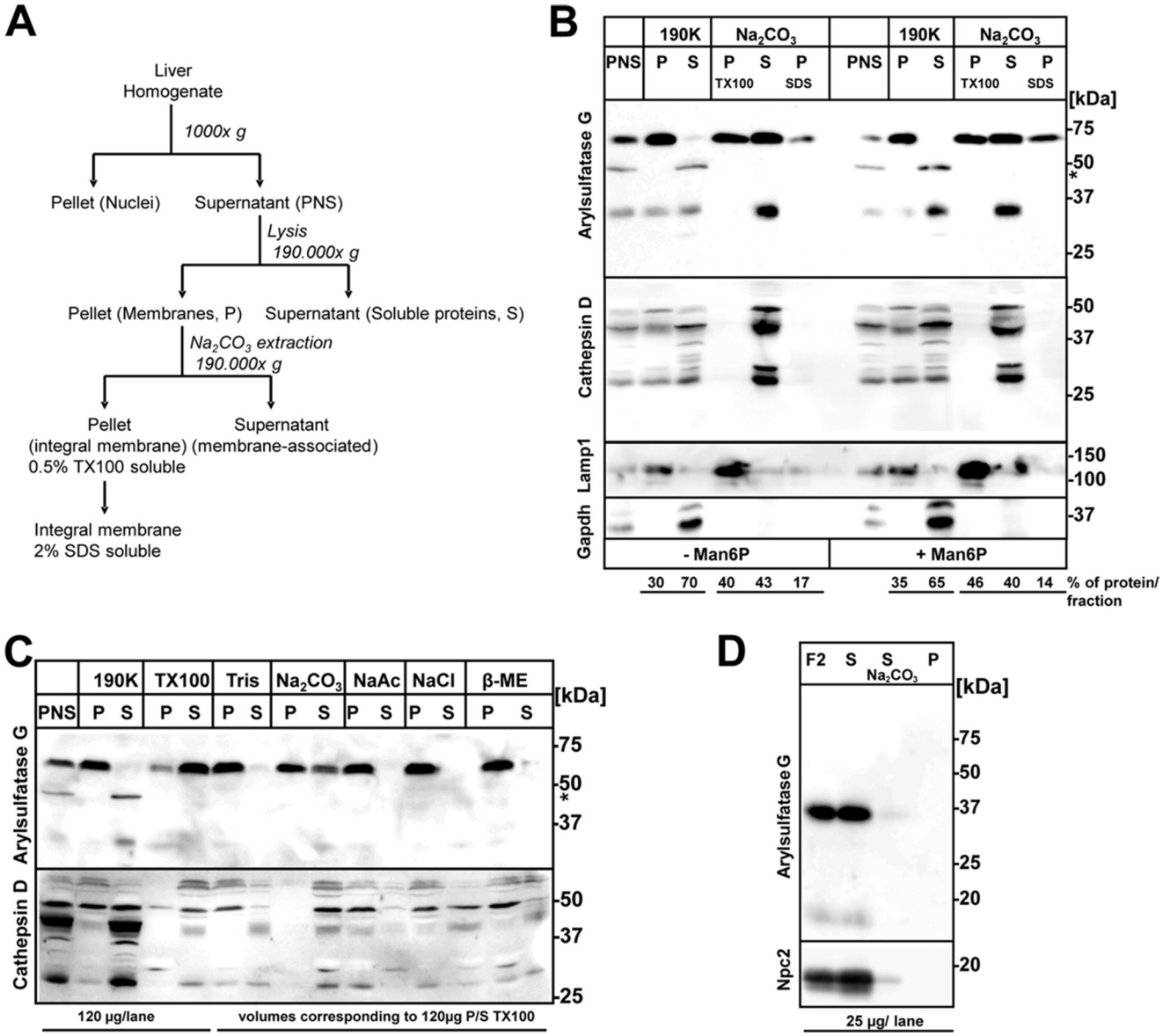

FIGURE 4. **Precursor of ARSG is tightly associated with membranes.** *A,* fractionation scheme for the separation of soluble proteins, membrane-associated proteins (Na_2CO_3 soluble), and integral membrane proteins from liver PNS. *B,* immunoblot analysis of all fractions derived from the membrane extraction procedure. Most of the ARSG precursor was found in the membrane fraction, whereas the 34-kDa fragment was almost completely soluble. Upon carbonate extraction of the membranes, residual membrane-associated 34-kDa fragment and parts of the precursor were extracted and detected in the supernatant upon centrifugation. Some precursor was only soluble after extraction with 0.5% Triton X-100 or even 2% SDS. The membrane association was independent of mannose 6-phosphate receptor binding, because addition of 5 mM Man6P to all buffers did not interfere with membrane association of ARSG. Cathepsin D was partially membrane-associated, but the remaining membranous portion was completely extractable with carbonate. Lamp1 and Gapdh were used as controls for integral membrane proteins and soluble proteins, respectively. 120 μg of PNS protein were loaded per lane. Protein distribution derived therefrom is shown at *bottom*. *C,* membrane association of the ARSG precursor was insensitive to acidic buffer (50 mM sodium acetate, pH 4.5), high salt buffer (1.5 M NaCl), or reducing buffer (TBS + 5 mM β-mercaptoethanol). Note loading of equal volumes corresponding to 120 μg of P/S from the Triton X-100 extraction. *D,* in contrast to the ARSG precursor, fractionation of tritosomes (F2) revealed quantitative extraction of both 34- and 18-kDa fragments in the soluble fraction. Niemann-Pick 2 protein (Npc2) is shown as a marker for a soluble lysosomal protein.

nine/cysteine pulse-chase analysis followed by immunoprecipitation (Fig. 5*A*). Because the endogenous ARSG could neither be immunoprecipitated sufficiently from MEF nor Neuro2a cells (data not shown), HT1080 cells transiently expressing tagged murine *mARSG* were used. Untransfected cells served as specificity controls because the antibody precipitated several nonspecific bands. Cells labeled for 1 h with [^{35}S]methionine/cysteine were either harvested (0-h chase) or chased for 2–72 h. After pulse labeling, only the 63-kDa ARSG precursor was observed. After 4 h of chase, both 34- and 18-kDa ARSG bands were detectable, and small amounts of an ~20-kDa polypeptide which might represent an intermediate form. Even after 72 h of chase, significant amounts of the 63-kDa ARSG precursor were still detectable. All molecular weight forms markedly disappeared after 24, 48, and 72 h, indicating a relatively short overall half-life.

To determine whether mouse and human ARSG orthologs are similarly processed, HT1080 cells were transfected in parallel either with human or murine *ARSG* cDNAs coding for RGS-His-tagged fusion proteins (Fig. 5*B*). Immunoblot detection with the RGS-His antibody revealed similar expression of

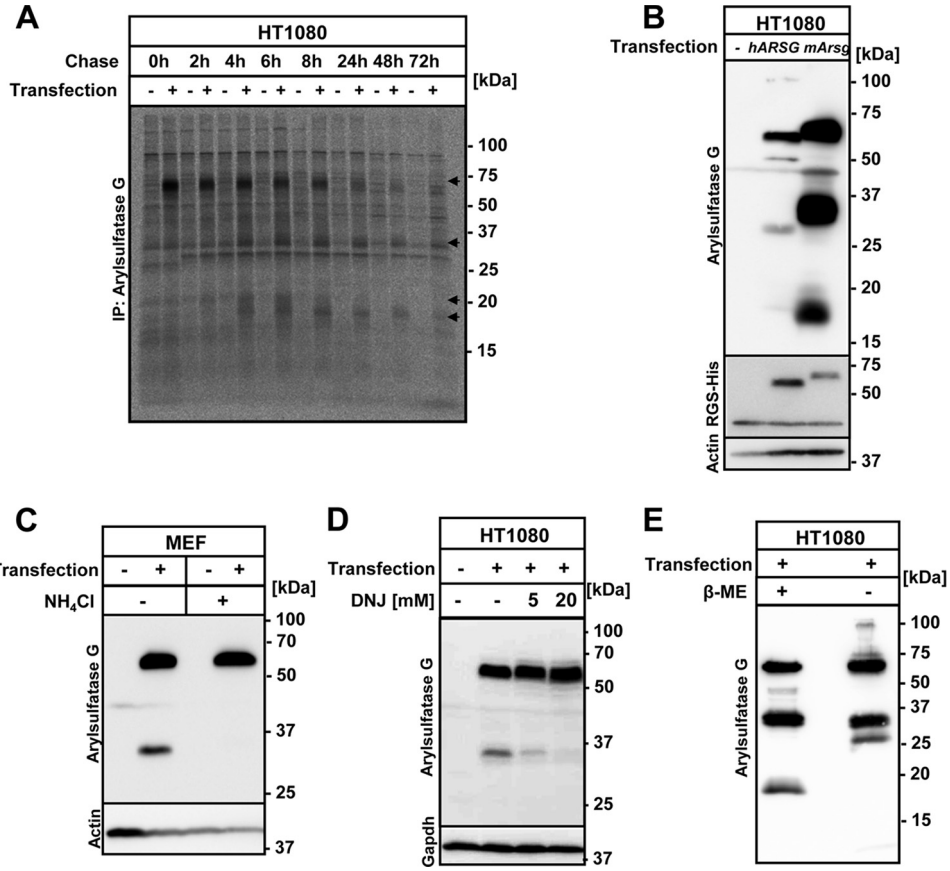

FIGURE 5. **Kinetics of proteolytic processing.** *A*, HT1080 cells were pulsed labeled with [^{35}S]methionine/cysteine for 1 h, harvested (0-h chase), or chased for the indicated time (0–72 h) followed by immunoprecipitation and autoradiography. Conversion of the 63-kDa precursor to processed fragments is apparent (see *arrowheads*), as is explained in the text. *B*, HT1080 cells were transfected with RGS-His-tagged human *ARSG* cDNA or murine *Arsg* cDNA, and expression was evaluated by immunoblotting. Immunoblot for RGS-His indicates similar transfection efficacy and expression of both cDNAs. Actin was used as a loading control. *C*, ARSG expressing MEFs were incubated with (+) or without (−) NH_4Cl after transfection and evaluated by immunoblot. *D*, HT1080 cells were analyzed by ARSG immunoblot after transfection and incubation in the presence and absence of 5 or 20 mM DNJ in the cell culture medium. Gapdh was used as a loading control. *E*, transfected HT1080 cells were analyzed by immunoblot under reducing (+ 1.5 M β-mercaptoethanol (+β-*ME*)) or nonreducing conditions (− β-mercaptoethanol (−β-*ME*)) revealing disulfide linkage of the 18-kDa chain to another ~10-kDa chain, as concluded from the newly appearing ~28-kDa band in the *right lane*.

both constructs. However, the RGS-His antibody exclusively detected the 63-kDa band, indicating removal of the C-terminal tag during processing. The ARSG antibody (raised against murine ARSG) cross-reacted with the human protein, but detection was much less efficient. Of note, using this antibody, a comparable processing pattern of both proteins was observed, even though differences in the extent of processing and subtle differences in the molecular weight of each chain became obvious between mouse and human ARSG.

To determine the intracellular compartment where processing takes place, ARSG-expressing MEF cells were incubated with the lysosomotropic drug NH_4Cl, an efficient inhibitor of lysosomal acidification. In the presence of NH_4Cl, delivery of newly synthesized acid hydrolases from the trans-Golgi network to endosomes is affected due to impaired dissociation of acid hydrolase-MPR complexes in late endosomes resulting in hypersecretion of lysosomal enzymes (31). Upon incubation of cells transiently expressing ARSG with NH_4Cl, no processed 34-kDa fragments were observed (Fig. 5*C*) indicating that ARSG processing occurred in post-Golgi compartments, most likely late endosomes/lysosomes. Similar results were obtained with mouse embryonic fibroblasts deficient for MPRs (MPR46 and MPR300) (32) and transfected with *mArsg* cDNA indicating the dependence of proper sorting of ARSG in the Golgi apparatus on MPRs in MEFs (data not shown).

To investigate the dependence of the transport of ARSG to post-ER compartments in HT1080 cells, the ER α-glucosidase inhibitor 1-deoxynojirmycin (33) was added to the cell culture medium at concentrations of 5 or 20 mM followed by transfection with *mArsg* cDNA. Proteolytic processing of ARSG was inhibited by deoxynojirimycin similar to NH_4Cl leading to an almost complete loss of the processed 34-kDa fragment (Fig. 5*D*) indicating that activity of ER glucosidases involved in *N*-glycan-dependent folding is critical for the efficient transport to the Golgi apparatus and subsequent delivery to lysosomes.

Finally, we evaluated the possibility of disulfide bridges between the different chains of ARSG (Fig. 5*E*). Immunoblot analysis of extracts from *ARSG*-transfected HT1080 cells under reducing (+β-mercaptoethanol) or nonreducing conditions (−β-mercaptoethanol) revealed a shift of the 18-kDa band ~28 kDa, indicating a disulfide bridge between the 18-kDa fragment and another smaller (~10-kDa) polypeptide, which is not detectable by immunoblotting but by pulse-chase experiments (see below and Fig. 6*A*). This disulfide bridge probably involves

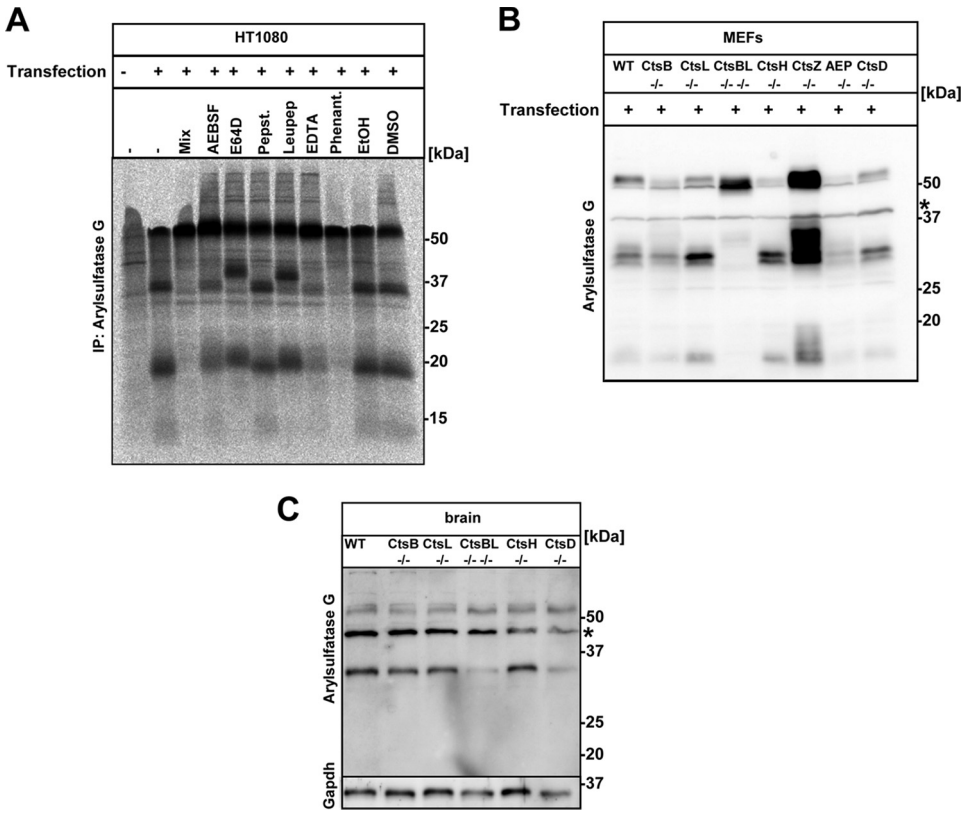

FIGURE 6. **Lysosomal cysteine proteases cathepsin B and cathepsin L mediate the processing of the ARSG precursor.** *A,* [^{35}S]methionine/cysteine pulse-chase analysis of stably *mArsg* transfected WT MEFs exposed to a mixture of different protease inhibitors and various inhibitors reveals impaired processing in E64D (cysteine protease inhibitor)- and leupeptin (*Leupep.*) (a general lysosomal inhibitor)-treated cells. Other inhibitors now show changes compared with vehicle-treated cells ((4-(2-aminoethyl)benzenesulfonyl fluoride (*AEBSF*), pepstatin (*Pepst.*), and EDTA) or completely abolished processing (phenanthroline (*Phenant.*)). *B,* stably mArsg-transfected MEFs derived from mice deficient for cathepsin B (*CtsB*$^{-/-}$), cathepsin L (*CtsL*$^{-/-}$), cathepsin B and L (*CtsB/L*$^{-/-}$), cathepsin Z (*CtsZ*), cathepsin H (*CtsH*$^{-/-}$), asparagine endopeptidase (*AEP*$^{-/-}$), and cathepsin D (*CtsD*$^{-/-}$) were analyzed by immunoblotting and showed impaired ARSG processing in *CtsB/L*$^{-/-}$ double-deficient cells. *C,* Western blot of brain homogenates shows reduced levels of the processed 34-kDa ARSG polypeptide band in double-deficient CtsB/L mice on the endogenous level.

Cys-195 of the 10-kDa chain, although there are several cysteine candidates in the 18-kDa chain (see below and Fig. 10). Gel filtration analysis of solubilized tritosomal fractions of wild type mice showed co-elution of the 34- and 18-kDa forms of ARSG, indicating an association between the two chains but absence of high molecular weight oligomers (data not shown).

Proteases Involved in Processing of ARSG—Our data indicated proteolytic processing of ARSG in late endosomal/lysosomal compartments. To characterize proteases responsible for the proteolytic cleavage of ARSG, a pulse-chase experiment was performed. HT1080 cells were transfected with the His-tagged mArsg construct for 16 h, metabolically labeled with [^{35}S]methionine/cysteine for 45 min, and subsequently incubated for 8 h with inhibitors for different classes of proteases (Fig. 6*A*). The first proteolytic cleavage of the 63-kDa precursor to generate the 44-kDa intermediate form was not affected by any of the used inhibitors, whereas further proteolytic processing into the 34- and 10-kDa fragments were efficiently prevented by leupeptin, a general inhibitor of cysteine, serine, and threonine peptidases, and E64D, a membrane-permeable cysteine protease inhibitor. To further define the responsible protease, we analyzed mARSG-expressing MEFs from different mouse strains deficient for cathepsin B, cathepsin L, cathepsin B and L, cathepsin H, cathepsin Z, cathepsin D, and asparagine endopeptidase/legumain by immunoblotting (Fig. 6*B*). Although differences in the total ARSG expression levels observed were caused by variable transfection efficiencies, the overall processing pattern was similar with the exception of cathepsin B/L double-deficient MEFs lacking essentially the processed 34- and 18-kDa fragments but revealed an additional faint band at ~44-kDa. These data indicate that both cathepsin L and B contribute to processing of ARSG. However, immunoblot analysis of brains (Fig. 6*C*) from the different cathepsin KO mouse strains still showed small amounts of the endogenous proteolytically processed 34-kDa ARSG band.

Transport of ARSG—Most soluble lysosomal proteins are modified with Man-6-P residues in the Golgi apparatus by the *N*-acetylglucosamine-1-phosphotransferase complex encoded by *Gnptab* and *Gnptg*. Man-6-P mediates their sorting in the Golgi apparatus by binding to Man-6-P-specific receptors and delivery to endosomes where MPRs release their cargo due to the acidic pH (34). The ARSG membrane association experiments (Fig. 4), however, suggested Man-6-P-independent membrane association implicating a Man-6-P-independent mode of transport. We therefore evaluated *Gnptab*-deficient mice for the presence of ARSG in lysosomes (Fig. 7*A*). Surprisingly, ARSG levels were even increased in tritosomes derived from these Man-6-P-deficient mice, indeed indicating the Man-6-P-independent mode of transport in hepatic cells. Alternative transport receptors were recently shown to be sortilin (encoded

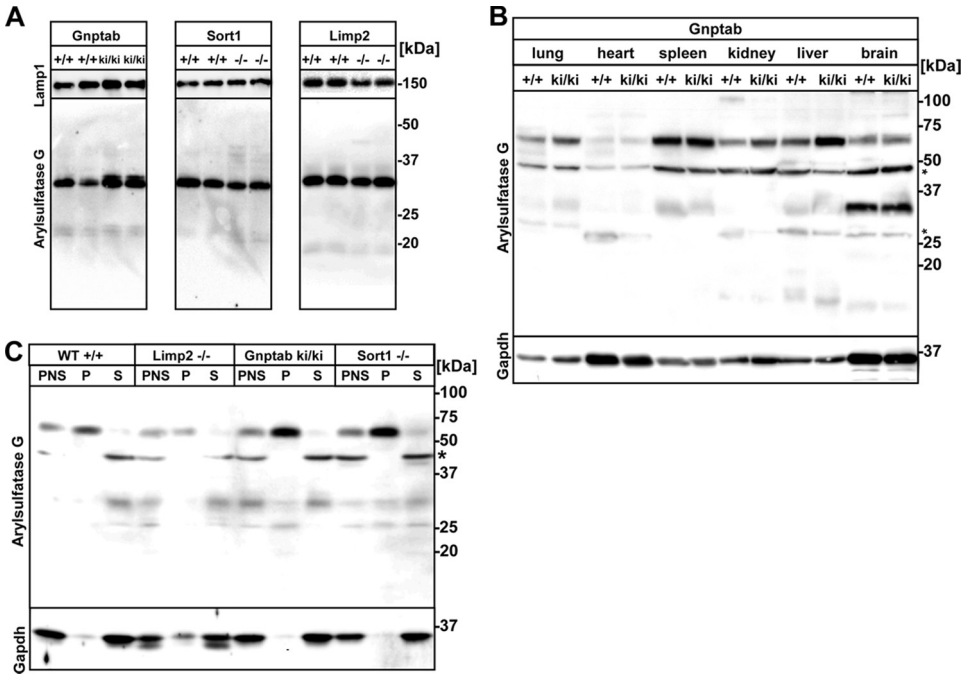

FIGURE 7. **Lysosomal transport of ARSG in the liver is independent of Man-6-P, sortilin, and Limp2.** *A,* tritosomes from WT, *Gnptab*$^{ki/ki}$, sortilin$^{-/-}$, and Limp2$^{-/-}$ mice were analyzed by ARSG immunoblotting and revealed similar or even increased levels of both lysosomal 34- and 18-kDa ARSG forms, indicating lysosomal transport in each respective genotype. Lamp1 is used as a loading control (40 μg protein/lane). *B,* tissue homogenates from WT$^{+/+}$ and *Gnptab*$^{ki/ki}$ knock-in mice were analyzed by ARSG immunoblotting and revealed similar or even increased levels of the precursor form of ARSG but similar levels of the processed form. *C,* membrane association of 63-kDa precursor ARSG form in the pellet fraction (*P*) independent of Man-6-P, Sort1, or Limp-2. Gapdh was used as a loading control. (120 μg of protein/lane).

by *Sort1*) and Limp2 (35–39). However, similar ARSG levels were found in tritosomes derived from Sort1 or Limp2 KO mice compared with appropriate wild type controls, indicating that lysosomal transport occurred independent of these alternative transport systems (Fig. 7*A*). Additionally, ARSG expression in various tissues of *Gnptab*-defective mice was compared with a wild type control. Similar levels of the processed ARSG band were observed in spleen, liver, and brain, whereas a slight increase in the amounts of the precursor was detected in lung, kidney, and liver, indicating Man-6-P-independent transport in these tissues (Fig. 7*B*). We failed to detect ARSG specifically in plasma (data not shown). We also evaluated the membrane association of ARSG in these receptors and Man-6-P mice (Fig. 7*C*). ARSG association with liver membranes was present in all genotypes, indicating only weak or no steady-state binding to MPRs, sortilin, or Limp2.

Glycosylation of ARSG—Overexpressed human ARSG was previously shown to be glycosylated (3). Because only tagged ARSG was evaluated, the glycosylation pattern of the processed forms escaped analysis due to cleavage of the tag. Treatment of liver PNS and lysosomal F2 fractions with PNGaseF or EndoH (Fig. 8*A*) revealed complete susceptibility of the precursor form of ARSG to both glycosidases, indicating high mannose-type glycosylation. In contrast, the 34-kDa proteolytically processed form was only marginally sensitive to EndoH treatment but fully susceptible to PNGaseF, indicating modification of some glycans to the complex type. We conclude that the 34-kDa form must have passed the Golgi apparatus, whereas the 63-kDa precursor could represent a pre-Golgi intermediate.

To identify the glycosylated asparagine residues, site-directed mutagenesis of the four potential *N*-glycosylation sites of murine ARSG was carried out followed by expression analysis of mutant ARSG in HT1080 cells (Fig. 8*B*). The exchange of Asn-117 to glutamine resulted in a molecular mass reduction of the 18-kDa chain, whereas the electrophoretic mobility of the 34-kDa polypeptide was not affected, indicating glycosylation of Asn-117 that is localized on the 18-kDa chain. No molecular mass differences between WT ARSG and ARSG N215Q mutant were observed under reducing conditions. However, under nonreducing conditions, the 28-kDa form of ARSG N215Q migrated with the same electrophoretic mobility as observed for the N117Q mutant, indicating glycosylation of Asn-215 and localization on the 10-kDa chain that is detectable by the ARSG antibody only when disulfide-bonded to the 18-Da chain (Fig. 5*E*). When Asn-356 was mutated (Fig. 8*B*), a clear shift in molecular mass of the 34-kDa ARSG form was observed demonstrating its use as a glycosylation site. The exchange of Asn-497 almost completely abolished proteolytic processing of ARSG presumably due to mis-sorting of this variant to the medium, at least in the HT1080 cells used, or impaired folding as indicated by a higher molecular weight band. These results demonstrate that all predicted *N*-glycosylation sites are used. Furthermore, the absence of processed ARSG forms implicates Man-6-P-dependent mode of transport in HT1080 cells.

Influence of Processing on ARSG Activity—To evaluate a putative activation after proteolytic processing, we determined the activity of the different molecular forms of ARSG against the pseudosubstrate pNCS. Activation of lysosomal enzymes by processing was described for several cathepsins, which require removal of inhibitory propeptides (40). Although ARSG is active against pNCS, this substrate is also cleaved by other much more abundant sulfatases. To measure specific ARSG

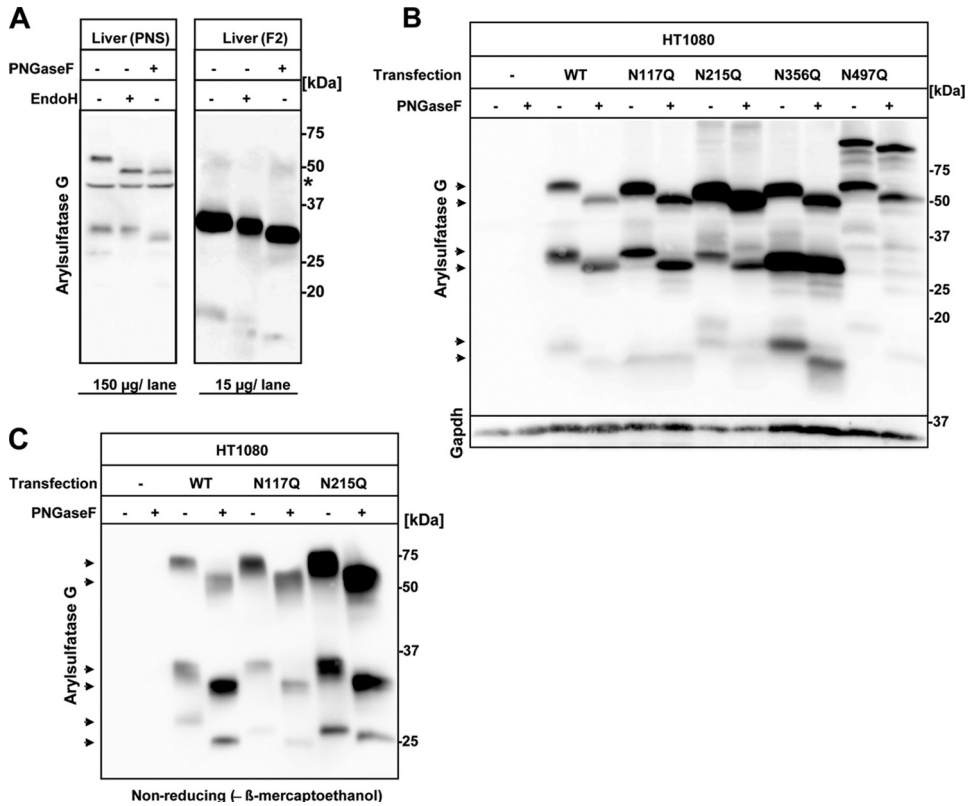

FIGURE 8. **Glycosylation pattern of the precursor and the processed forms of ARSG are different.** *A,* PNS and lysosomal F2 fractions were treated with PNGaseF and EndoH, respectively, and analyzed by immunoblotting. Whereas the precursor is completely EndoH-sensitive, both processed forms (34- and 18-kDa) are only partially sensitive to EndoH, indicating at least a partial complex-type glycosylation. *B,* HT1080 cells were transfected with wild type or mutant m*Arsg* cDNAs, each of the four Asn-Xaa-(Ser/Thr) (where Xaa is not proline) glycosylation motifs, as indicated and analyzed by immunoblotting under reducing conditions. Incubation of cell lysates with or without PNGase F indicated use of all four glycosylation sites and their localization on the three chains of processed ARSG (see text). *C,* HT1080 cells stably expressing WT ARSG or mutants N117Q and N215Q were harvested and lysed in the presence of *N*-ethylmaleimide. One aliquot of each cell lysate was treated with PNGase F under nonreducing conditions, and another aliquot remained untreated. In the untreated samples, the 28-kDa ARSG form, composed of the 18- and 10-kDa ARSG chains, showed a reduced molecular weight in the two mutants in comparison with WT ARSG, indicating that both *N*-glycosylation sites are located on the 28-kDa polypeptide, with Asn-117 being located on the 18-kDa chain.

activity, we immunoprecipitated endogenous ARSG followed by the pNCS assay. ARSG activity was linear after immunoprecipitation from liver extracts corresponding to a range of 0.5–2.5 mg of total protein (Fig. 9*A*), indicating sufficient antibody binding capacity in this range. The comparison of homogenates of different organs, including brain, liver, and testis, revealed significant differences in the hydrolysis of pNCS (Fig. 9*B*). However, these differences matched the amounts of immunoreactive ARSG (data not shown), suggesting little or no influence of ARSG processing on activity. Tissues from ARSG-deficient mice showed no activity against pNCS, highlighting the specificity of our assay. Subjecting similar amounts of the pre-lysosomal 63-kDa precursor form and the processed lysosomal mature 34-kDa form, as determined by immunoblot (Fig. 9*C*, *right panel*), both from liver differential centrifugation (Fig. 2), to our immunoprecipitation-based assay revealed a slight increase in the activity of the processed lysosomal form, again proportional to the slightly higher amounts of the applied 34-kDa form. These data clearly show that proteolytic cleavage of ARSG has little or no influence on its activity toward the pNCS substrate.

DISCUSSION

The human and mouse genomes encode eight sulfatases for which a lysosomal localization has been demonstrated. Two of these sulfatases, arylsulfatase K and ARSG, have been described and characterized only recently after heterologous ectopic expression (2, 3). In this study, detailed biochemical description of the endogenous ARSG enzyme is presented to understand *in vivo* expression, function, and properties of this enzyme, which is critical for the degradation of 3-*O*-sulfated glucosamine residues of heparan sulfate.

ARSG is broadly expressed in several tissues. However, marked differences were determined by immunoblot analyses. Previous RT-PCR analyses of murine tissues revealed the highest mRNA expression in the lung and only moderate expression in liver and spleen (41). In contrast, no *ARSG* transcripts were found in the human lung, but high expression levels were found in human liver and spleen (3). At the protein level, we found the highest expression in mouse brain, kidney, testis, liver, and spleen. These apparent discrepancies might be explained by both species-specific differences and differences in post-transcriptional regulation of mRNAs or the stability of the protein. Interestingly, ARSG protein levels correlate well with the distribution of 3-*O*-sulfated heparan sulfate in the KO mouse, which is highest in brain, liver, and kidney (7), indicating precisely regulated expression in tissues with high substrate turnover rather than ubiquitous expression with characteristics of a "housekeeping" gene.

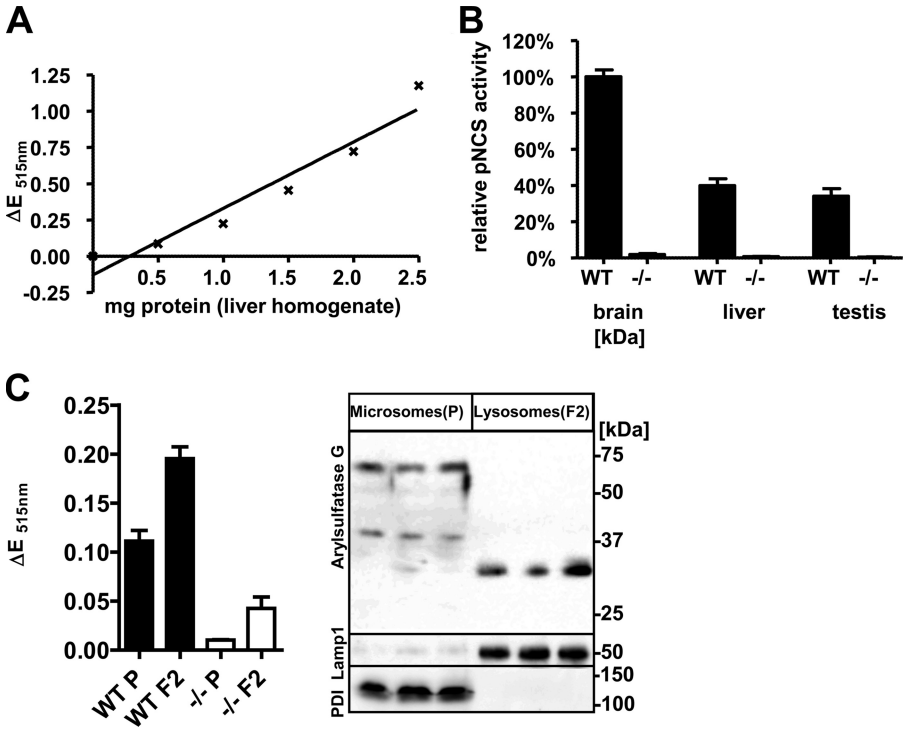

FIGURE 9. **Development of an ARSG-specific activity assay and influence of proteolytic processing on ARSG activity.** *A*, immunoprecipitation of ARSG from increasing amounts of lysed liver PNS followed by colorimetric sulfatase activity assay with the pseudosubstrate pNCS shows a linear increase of pNCS turnover up to 2.5 mg of PNS protein, indicating no antibody limitation in the selected range. (ΔE = change of pNCS product absorbance measured at 515 nm). *B*, ARSG activity measurement with the above-described IP-based assays with 2 mg of protein of different organ extracts from wild type and *Arsg* KO mice (n = 3) and 4 μl of ARSG antibody revealed marginal background activity in tissues of KO mice, indicating high specificity of the assay. Highest activity can be observed in brain homogenates. *C*, IP-based ARSG activity assay of 300 μg of liver microsomal fraction (P) and 30 μg of lysosomal fraction F2 from three WT mice (*left panel*). The higher activity in the F2 fraction corresponded to the higher amount of the 34-kDa processed ARSG form as compared with the 63-kDa precursor in the microsomal fraction (*right panel*), hence indicating comparable or only slightly increased activity of processed ARSG.

In addition to differences in the expression level, this study demonstrates that ARSG undergoes proteolytic processing during maturation to a three-chain form in a tissue-dependent manner. In this respect ARSG resembles other lysosomal sulfatases, including iduronate-2-sulfatase (42), sulfamidase (43, 44), arylsulfatase A (45), arylsulfatase B (46), *N*-acetylgalactosamine-6-sulfatase (47), and *N*-acetylglucosamine-6-sulfatase (48), which were similarly shown to be proteolytically processed. Our pulse-chase analyses exclude translation of possible shorter mRNA splice variants, which are annotated in databases resulting in truncated ARSG form(s). They rather showed a complex maturation process of the 63-kDa ARSG precursor protein to 34-, 18-, and 10-kDa chains (Fig. 10), which relies on transport to lysosomes, low pH, and lysosomal proteases. The inhibitor and expression experiments revealed that lysosomal cysteine proteases, which are sensitive to E64D, and our transfection experiments using protease-deficient MEFs revealed that cathepsin B and L play an important role in the processing step cleaving a 44-kDa intermediate into the 34- and 10-kDa chains. However, E64D only partially inhibited processing suggesting either incomplete inhibition of the responsible protease(s) or the possibility that the activity of another protease depends on cathepsin B and L. This alternative explanation could also explain the occurrence of proteolytic processing in the brain of cathepsin B/L double-deficient mice (Fig. 6*C*).

Interestingly, subcellular fractionation experiments exhibit a relatively long lasting stability of the endogenous ARSG precursor protein in a pre-lysosomal compartment, with the precursor co-fractionating with Pdi, an ER-resident protein. In the liver, most ARSG was detected, at steady state, in its precursor form. Finally, our deglycosylation analysis demonstrated mostly a high mannose-type glycosylation of the 63-kDa precursor, whereas the proteolytically processed ARSG carried complex-type *N*-glycans. This indicates that the forms that become processed in late endosomes had passed the Golgi apparatus, although the precursor is a pre-Golgi intermediate (49).

All these lines of evidence indicate that ARSG is not only present in the endo-/lysosomal compartment but to significant amounts also in pre-lysosomal compartments like the ER. Interestingly, in the first report on ARSG, its subcellular localization was assigned to the ER (41). However, these studies were conducted under overexpressing conditions that are often accompanied by ER accumulation due to folding stress. Furthermore, detection was carried out with an antibody against an epitope tag, which is rapidly removed during maturation, as also seen in this study, and hence it precludes detection of the mature forms in acidic compartments. Our experimental setup aimed to detect endogenous protein wherever possible, excluding potential overexpression artifacts. It confirms a partial ER localization, described in this initial study, at least for the ARSG precursor. Nevertheless, our subcellular fractionation experiments unambiguously reveal a lysosomal localization of functional and active ARSG, which is in line with the lysosomal accumulation of GAGs upon ablation of ARSG in the KO

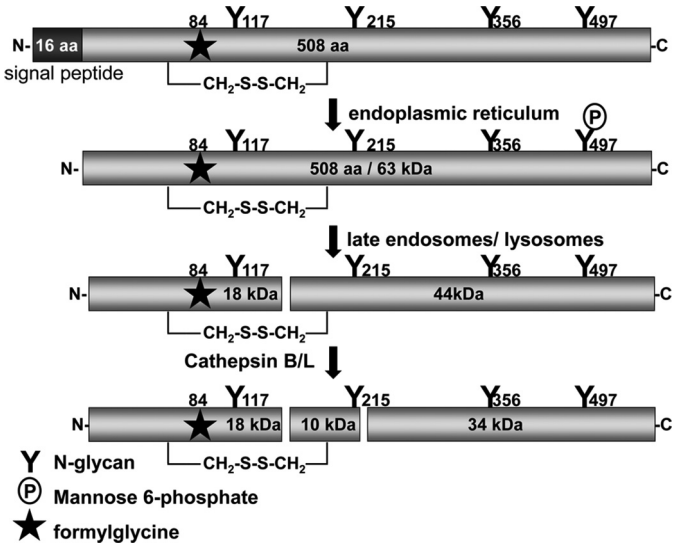

FIGURE 10. **Proposed processing scheme for ARSG.** ARSG is synthesized as a pre-precursor protein with a predicted signal peptide comprising 16 amino acids. In the ER, the signal peptide is cleaved off co-translationally, and cysteine in position 84 is modified to formylglycine, and asparagine residues are modified with *N*-glycans at positions 117, 215, 356, and 497. In the Golgi apparatus, *N*-glycans become partially modified to complex-type or mannose-type glycans, from which Asn-497 becomes modified with mannose 6-phosphate. *En route* to late endosomes/lysosomes, proteolytic processing takes place in two steps, yielding two fragments in the first step (apparent molecular masses of 44 and 18 kDa). In the second step, the 44-kDa fragment is processed further to the 34- and 10-kDa chains. The 10-kDa chain is a cleavage product of the 44-kDa fragment but linked to the 18-kDa chain through a disulfide bridge, as found after analysis by nonreducing gel electrophoresis (see Fig. 5*E*). According to the three-dimensional homology model for ARSG, based on its closest relative arylsulfatase A (Protein Data Bank code 1E2S), the two processing sites are located in surface-exposed loop regions (approximate amino acid positions 182–192 and 255–268, respectively). Accordingly, Cys-195 is the only cysteine located on the 10-kDa chain and hence disulfide-bridged to either Cys-167, -178 or -181 on the 18-kDa chain.

mice. The relevance of the slow transport kinetics of ARSG, causing precursor accumulation in microsomal compartments, remains unknown. The low residual activity of ARSG at neutral pH (3) makes a second GlcNS3S-unrelated hydrolytic activity in the ER highly unlikely.

Our biochemical studies revealed, beside the unexpectedly long residency in the ER, a strong association of the 63-kDa precursor protein, but not of processed ARSG, with cellular membranes as shown by lysis of organelles followed by ultracentrifugation. Of note, ARSG does not contain any predicted transmembrane domain. The membrane association was only partially lost after incubation with carbonate and unaffected by Man-6-P, high salt, reducing agent, or acidic buffers. Because the precursor protein is quantitatively associated with membranes, it can be concluded that the membrane-associated fraction is completely localized to the ER. The strong membrane association of the precursor and the loss of membrane association of the processed chains raise the question regarding how ARSG is retained in the ER and whether the putative interaction with an ER resident protein is important for its mode of transport. The lack of proteolytic processing upon incubation of cells with the glucosidase inhibitor 1-deoxynojirmycin may result from inappropriate folding or its abnormal interaction with receptors in the endoplasmic reticulum and thus prolonged interaction with quality control chaperones like calnexin. Whether such interaction is the reason for the rather slow itinerary of ARSG through the ER also in the absence of 1-deoxynojirmycin remains to be investigated.

In fact, our subcellular fractionation studies revealed equal or even higher levels of processed ARSG in liver lysosomes of *Gnptab* knock-in mice (with a defect in the generation of Man-6-P), sortilin-, and also Limp2-deficient mice compared with corresponding controls. A similar observation was made in other tissues of *Gnptab* knock-in mice, which revealed no differences or even increased levels in the steady-state levels of ARSG. Thus, two independent modes of transport seem to be operative in the liver and other tissues, of which one is obviously independent of Man-6-P and another pathway compensates for the deficiency of these known receptors for lysosomal proteins and Man-6-P. These data are in line with a series of other lysosomal enzymes, for which Man-6-P-independent transport was shown and, interestingly, membrane association as well. These include cathepsin D, prosaposin, and glucocerebrosidase (28, 29, 50, 51). Even though for the latter, Limp2 binding and a Limp2-dependent mode of transport was shown (35), we can exclude that pathway because ARSG levels were similar in lysosomes from WT and Limp2-deficient mice and membrane association was not lost in liver membranes of Limp2 KOs. We are currently trying to identify interaction partners of ARSG, which might give insight into a new transport route. Furthermore, a likely explanation could also involve a secretion of ARSG into the bloodstream and (Man-6-P-independent) re-uptake mechanism, which was previously suggested to act as a compensatory mechanism in MPR-double deficient mouse (52). However, we failed to detect ARSG in the plasma of mice, preventing experimental proof for this hypothesis.

Remarkably, in MPR-deficient MEFs ARSG is not proteolytically processed, implicating mis-sorting and thereby different transport routes in fibroblasts and other tissues like liver, as described previously for other lysosomal soluble enzymes in MPR double deficient mice (52). Furthermore, mutation of asparagine 497 considerably abrogated processing and most likely transport to lysosomes in HT1080 cells. In good agreement with our data, this residue was previously shown to be Man-6-P-modified in a screen for Man-6-P modification of lysosomal proteins (53). Because all other glycosylation site mutants were processed properly, this residue is likely the only Man-6-P-modified sorting signal.

Proteolytic processing was shown to be critical for maximal activity for some lysosomal enzymes or even activation in general, although it was shown to be dispensable for others (40, 54–60). We therefore aimed to investigate a possible activation of the hydrolytic activity by proteolytic processing. Even though our IP-based assay might be biased to some extent by different efficiencies of precipitation of the used polyclonal antibody, which was raised against the full-length recombinant protein, or of the different ARSG forms (precursor and processed), we can exclude a substantial gain of activity due to processing. This observation is further strengthened by our previous results, which indicated that the precursor is already active against both the pseudosubstrates pNCS and 4-methylumbelliferyl sulfate (3) and also the natural substrate GlcNS3S (7). We are currently developing an assay based on the degra-

dation of the natural substrate GlcNS3S for the determination of endogenous ARSG activity, which is independent of any immunological reagents and thus will be useful for further characterization of ARSG and to find putative MPS patients with ARSG deficiency. It should be noted, however, that diagnosis of ARSG deficiency as a lysosomal storage disorder most probably will have to take into consideration the existence of an extra-lysosomal ARSG form under physiological and probably also under pathological steady-state conditions that contributes to the measured cellular activity.

Acknowledgments—We thank Claudia Prange and Marion Knufinke for excellent technical assistance. Limp2-deficient mice were a kind gift from Paul Saftig. Sortilin knock-out mice were kindly provided by Maximiliano G. Gutierrez and Anders Nykjaer. Npc2-antiserum was a gift from Shutish Patel. Rab5 antibody was a kind gift from Gabriele Fischer von Mollard.

REFERENCES

1. Sardiello, M., Annunziata, I., Roma, G., and Ballabio, A. (2005) Sulfatases and sulfatase modifying factors: an exclusive and promiscuous relationship. *Hum. Mol. Genet.* **14,** 3203–3217
2. Wiegmann, E. M., Westendorf, E., Kalus, I., Pringle, T. H., Lübke, T., and Dierks, T. (2013) Arylsulfatase K, a novel lysosomal sulfatase. *J. Biol. Chem.* **288,** 30019–30028
3. Frese, M. A., Schulz, S., and Dierks, T. (2008) Arylsulfatase G, a novel lysosomal sulfatase. *J. Biol. Chem.* **283,** 11388–11395
4. Diez-Roux, G., and Ballabio, A. (2005) Sulfatases and human disease. *Annu. Rev. Genomics Hum. Genet.* **6,** 355–379
5. Mehl, E., and Jatzkewitz, H. (1968) Cerebroside 3-sulfate as a physiological substrate of arylsulfatase A. *Biochim. Biophys. Acta* **151,** 619–627
6. Muenzer, J. (2004) The mucopolysaccharidoses: a heterogeneous group of disorders with variable pediatric presentations. *J. Pediatr.* **144,** S27–S34
7. Kowalewski, B., Lamanna, W. C., Lawrence, R., Damme, M., Stroobants, S., Padva, M., Kalus, I., Frese, M. A., Lübke, T., Lüllmann-Rauch, R., D'Hooge, R., Esko, J. D., and Dierks, T. (2012) Arylsulfatase G inactivation causes loss of heparan sulfate 3-*O*-sulfatase activity and mucopolysaccharidosis in mice. *Proc. Natl. Acad. Sci. U.S.A.* **109,** 10310–10315
8. Abitbol, M., Thibaud, J. L., Olby, N. J., Hitte, C., Puech, J. P., Maurer, M., Pilot-Storck, F., Hédan, B., Dréano, S., Brahimi, S., Delattre, D., André, C., Gray, F., Delisle, F., Caillaud, C., Bernex, F., Panthier, J. J., Aubin-Houzelstein, G., Blot, S., and Tiret, L. (2010) A canine arylsulfatase G (ARSG) mutation leading to a sulfatase deficiency is associated with neuronal ceroid lipofuscinosis. *Proc. Natl. Acad. Sci. U.S.A.* **107,** 14775–14780
9. Gamp, A. C., Tanaka, Y., Lüllmann-Rauch, R., Wittke, D., D'Hooge, R., De Deyn, P. P., Moser, T., Maier, H., Hartmann, D., Reiss, K., Illert, A. L., von Figura, K., and Saftig, P. (2003) LIMP-2/LGP85 deficiency causes ureteric pelvic junction obstruction, deafness and peripheral neuropathy in mice. *Hum. Mol. Genet.* **12,** 631–646
10. Kollmann, K., Damme, M., Markmann, S., Morelle, W., Schweizer, M., Hermans-Borgmeyer, I., Röchert, A. K., Pohl, S., Lübke, T., Michalski, J. C., Käkelä, R., Walkley, S. U., and Braulke, T. (2012) Lysosomal dysfunction causes neurodegeneration in mucolipidosis II 'knock-in' mice. *Brain* **135,** 2661–2675
11. Nykjaer, A., Lee, R., Teng, K. K., Jansen, P., Madsen, P., Nielsen, M. S., Jacobsen, C., Kliemannel, M., Schwarz, E., Willnow, T. E., Hempstead, B. L., and Petersen, C. M. (2004) Sortilin is essential for proNGF-induced neuronal cell death. *Nature* **427,** 843–848
12. Halangk, W., Lerch, M. M., Brandt-Nedelev, B., Roth, W., Ruthenbuerger, M., Reinheckel, T., Domschke, W., Lippert, H., Peters, C., and Deussing, J. (2000) Role of cathepsin B in intracellular trypsinogen activation and the onset of acute pancreatitis. *J. Clin. Invest.* **106,** 773–781
13. Bühling, F., Kouadio, M., Chwieralski, C. E., Kern, U., Hohlfeld, J. M., Klemm, N., Friedrichs, N., Roth, W., Deussing, J. M., Peters, C., and Reinheckel, T. (2011) Gene targeting of the cysteine peptidase cathepsin H impairs lung surfactant in mice. *PLoS One* **6,** e26247
14. Roth, W., Deussing, J., Botchkarev, V. A., Pauly-Evers, M., Saftig, P., Hafner, A., Schmidt, P., Schmahl, W., Scherer, J., Anton-Lamprecht, I., Von Figura, K., Paus, R., and Peters, C. (2000) Cathepsin L deficiency as molecular defect of furless: hyperproliferation of keratinocytes and perturbation of hair follicle cycling. *FASEB J.* **14,** 2075–2086
15. Matthews, S. P., Werber, I., Deussing, J., Peters, C., Reinheckel, T., and Watts, C. (2010) Distinct protease requirements for antigen presentation *in vitro* and *in vivo*. *J. Immunol.* **184,** 2423–2431
16. Saftig, P., Hetman, M., Schmahl, W., Weber, K., Heine, L., Mossmann, H., Köster, A., Hess, B., Evers, M., and von Figura, K. (1995) Mice deficient for the lysosomal proteinase cathepsin D exhibit progressive atrophy of the intestinal mucosa and profound destruction of lymphoid cells. *EMBO J.* **14,** 3599–3608
17. Claussen, M., Kübler, B., Wendland, M., Neifer, K., Schmidt, B., Zapf, J., and Braulke, T. (1997) Proteolysis of insulin-like growth factors (IGF) and IGF-binding proteins by cathepsin D. *Endocrinology* **138,** 3797–3803
18. Fischer von Mollard, G., Stahl, B., Walch-Solimena, C., Takei, K., Daniels, L., Khoklatchev, A., De Camilli, P., Südhof, T. C., and Jahn, R. (1994) Localization of Rab5 to synaptic vesicles identifies endosomal intermediate in synaptic vesicle recycling pathway. *Eur. J. Cell Biol.* **65,** 319–326
19. Ong, W. Y., Sundaram, R. K., Huang, E., Ghoshal, S., Kumar, U., Pentchev, P. G., and Patel, S. C. (2004) Neuronal localization and association of Niemann Pick C2 protein (HE1/NPC2) with the postsynaptic density. *Neuroscience* **128,** 561–570
20. Schuermann, M. (1990) An expression vector system for stable expression of oncogenes. *Nucleic Acids Res.* **18,** 4945–4946
21. Kollmann, K., Damme, M., Deuschl, F., Kahle, J., D'Hooge, R., Lüllmann-Rauch, R., and Lübke, T. (2009) Molecular characterization and gene disruption of mouse lysosomal putative serine carboxypeptidase 1. *FEBS J.* **276,** 1356–1369
22. Gieselmann, V., Pohlmann, R., Hasilik, A., and Von Figura, K. (1983) Biosynthesis and transport of cathepsin D in cultured human fibroblasts. *J. Cell Biol.* **97,** 1–5
23. Fujiki, Y., Hubbard, A. L., Fowler, S., and Lazarow, P. B. (1982) Isolation of intracellular membranes by means of sodium carbonate treatment: application to endoplasmic reticulum. *J. Cell Biol.* **93,** 97–102
24. Wattiaux, R., Wibo, M., and Baudhuin, P. (1963) Effect of the injection of Triton WR 1339 on the hepatic lysosomes of the rat. *Arch. Int. Physiol. Biochim.* **71,** 140–142
25. Deuschl, F., Kollmann, K., von Figura, K., and Lübke, T. (2006) Molecular characterization of the hypothetical 66.3-kDa protein in mouse: lysosomal targeting, glycosylation, processing and tissue distribution. *FEBS Lett.* **580,** 5747–5752
26. Merion, M., and Sly, W. S. (1983) The role of intermediate vesicles in the adsorptive endocytosis and transport of ligand to lysosomes by human fibroblasts. *J. Cell Biol.* **96,** 644–650
27. Storrie, B., Pool, R. R., Jr., Sachdeva, M., Maurey, K. M., and Oliver, C. (1984) Evidence for both prelysosomal and lysosomal intermediates in endocytic pathways. *J. Cell Biol.* **98,** 108–115
28. Rijnboutt, S., Kal, A. J., Geuze, H. J., Aerts, H., and Strous, G. J. (1991) Mannose 6-phosphate-independent targeting of cathepsin D to lysosomes in HepG2 cells. *J. Biol. Chem.* **266,** 23586–23592
29. Rijnboutt, S., Aerts, H. M., Geuze, H. J., Tager, J. M., and Strous, G. J. (1991) Mannose 6-phosphate-independent membrane association of cathepsin D, glucocerebrosidase, and sphingolipid-activating protein in HepG2 cells. *J. Biol. Chem.* **266,** 4862–4868
30. Diment, S., Leech, M. S., and Stahl, P. D. (1988) Cathepsin D is membrane-associated in macrophage endosomes. *J. Biol. Chem.* **263,** 6901–6907
31. Braulke, T., Geuze, H. J., Slot, J. W., Hasilik, A., and von Figura, K. (1987) On the effects of weak bases and monensin on sorting and processing of lysosomal enzymes in human cells. *Eur. J. Cell Biol.* **43,** 316–321
32. Pohlmann, R., Boeker, M. W., and von Figura, K. (1995) The two mannose 6-phosphate receptors transport distinct complements of lysosomal proteins. *J. Biol. Chem.* **270,** 27311–27318
33. Lemansky, P., Gieselmann, V., Hasilik, A., and von Figura, K. (1984) Cathepsin D and β-hexosaminidase synthesized in the presence of 1-de-

oxynojirimycin accumulate in the endoplasmic reticulum. *J. Biol. Chem.* **259,** 10129–10135
34. Kollmann, K., Pohl, S., Marschner, K., Encarnação, M., Sakwa, I., Tiede, S., Poorthuis, B. J., Lübke, T., Müller-Loennies, S., Storch, S., and Braulke, T. (2010) Mannose phosphorylation in health and disease. *Eur. J. Cell Biol.* **89,** 117–123
35. Reczek, D., Schwake, M., Schröder, J., Hughes, H., Blanz, J., Jin, X., Brondyk, W., Van Patten, S., Edmunds, T., and Saftig, P. (2007) LIMP-2 is a receptor for lysosomal mannose-6-phosphate-independent targeting of β-glucocerebrosidase. *Cell* **131,** 770–783
36. Lefrancois, S., Zeng, J., Hassan, A. J., Canuel, M., and Morales, C. R. (2003) The lysosomal trafficking of sphingolipid activator proteins (SAPs) is mediated by sortilin. *EMBO J.* **22,** 6430–6437
37. Ni, X., and Morales, C. R. (2006) The lysosomal trafficking of acid sphingomyelinase is mediated by sortilin and mannose 6-phosphate receptor. *Traffic* **7,** 889–902
38. Ni, X., Canuel, M., and Morales, C. R. (2006) The sorting and trafficking of lysosomal proteins. *Histol. Histopathol.* **21,** 899–913
39. Wähe, A., Kasmapour, B., Schmaderer, C., Liebl, D., Sandhoff, K., Nykjaer, A., Griffiths, G., and Gutierrez, M. G. (2010) Golgi-to-phagosome transport of acid sphingomyelinase and prosaposin is mediated by sortilin. *J. Cell Sci.* **123,** 2502–2511
40. Nishimura, Y., Kawabata, T., and Kato, K. (1988) Identification of latent procathepsins B and L in microsomal lumen: characterization of enzymatic activation and proteolytic processing *in vitro*. *Arch. Biochem. Biophys.* **261,** 64–71
41. Ferrante, P., Messali, S., Meroni, G., and Ballabio, A. (2002) Molecular and biochemical characterisation of a novel sulphatase gene: Arylsulfatase G (ARSG). *Eur. J. Hum. Genet.* **10,** 813–818
42. Froissart, R., Millat, G., Mathieu, M., Bozon, D., and Maire, I. (1995) Processing of iduronate 2-sulphatase in human fibroblasts. *Biochem. J.* **309,** 425–430
43. Freeman, C., and Hopwood, J. J. (1986) Human liver sulphamate sulphohydrolase. Determinations of native protein and subunit M_r values and influence of substrate agylcone structure on catalytic properties. *Biochem. J.* **234,** 83–92
44. Bielicki, J., Hopwood, J. J., Melville, E. L., and Anson, D. S. (1998) Recombinant human sulphamidase: expression, amplification, purification and characterization. *Biochem. J.* **329,** 145–150
45. Fujii, T., Kobayashi, T., Honke, K., Gasa, S., Ishikawa, M., Shimizu, T., and Makita, A. (1992) Proteolytic processing of human lysosomal arylsulfatase A. *Biochim. Biophys. Acta* **1122,** 93–98
46. Bond, C. S., Clements, P. R., Ashby, S. J., Collyer, C. A., Harrop, S. J., Hopwood, J. J., and Guss, J. M. (1997) Structure of a human lysosomal sulfatase. *Structure* **5,** 277–289
47. Masue, M., Sukegawa, K., Orii, T., and Hashimoto, T. (1991) *N*-Acetylgalactosamine-6-sulfate sulfatase in human placenta: purification and characteristics. *J. Biochem.* **110,** 965–970
48. Freeman, C., Clements, P. R., and Hopwood, J. J. (1987) Human liver *N*-acetylglucosamine-6-sulphate sulphatase. Purification and characterization. *Biochem. J.* **246,** 347–354
49. Aebi, M. (2013) *N*-Linked protein glycosylation in the ER. *Biochim. Biophys. Acta* **1833,** 2430–2437
50. Nishimura, Y., and Himeno, M. (1995) Cathepsin D associates with lysosomal membranous protein. *Biol. Pharm. Bull.* **18,** 1340–1346
51. Zhu, Y., and Conner, G. E. (1994) Intermolecular association of lysosomal protein precursors during biosynthesis. *J. Biol. Chem.* **269,** 3846–3851
52. Dittmer, F., Hafner, A., Ulbrich, E. J., Moritz, J. D., Schmidt, P., Schmahl, W., Pohlmann, R., and Figura, K. V. (1998) I-cell disease-like phenotype in mice deficient in mannose 6-phosphate receptors. *Transgenic Res.* **7,** 473–483
53. Sleat, D. E., Zheng, H., Qian, M., and Lobel, P. (2006) Identification of sites of mannose 6-phosphorylation on lysosomal proteins. *Mol. Cell. Proteomics* **5,** 686–701
54. Ljusberg, J., Wang, Y., Lång, P., Norgård, M., Dodds, R., Hultenby, K., Ek-Rylander, B., and Andersson, G. (2005) Proteolytic excision of a repressive loop domain in tartrate-resistant acid phosphatase by cathepsin K in osteoclasts. *J. Biol. Chem.* **280,** 28370–28381
55. Huang, R. T., Liao, T. H., and Lu, S. C. (2009) Proteolytic processing of porcine deoxyribonuclease II occurs in lysosomes but is not required for enzyme activation. *FEBS J.* **276,** 1891–1899
56. Zhao, L. Y., Tsuboi, K., Okamoto, Y., Nagahata, S., and Ueda, N. (2007) Proteolytic activation and glycosylation of *N*-acylethanolamine-hydrolyzing acid amidase, a lysosomal enzyme involved in the endocannabinoid metabolism. *Biochim. Biophys. Acta* **1771,** 1397–1405
57. Durand, S., Feldhammer, M., Bonneil, E., Thibault, P., and Pshezhetsky, A. V. (2010) Analysis of the biogenesis of heparan sulfate acetyl-CoA:α-glucosaminide *N*-acetyltransferase provides insights into the mechanism underlying its complete deficiency in mucopolysaccharidosis IIIC. *J. Biol. Chem.* **285,** 31233–31242
58. Cohen, E., Atzmon, R., Vlodavsky, I., and Ilan, N. (2005) Heparanase processing by lysosomal/endosomal protein preparation. *FEBS Lett.* **579,** 2334–2338
59. Golabek, A. A., Wujek, P., Walus, M., Bieler, S., Soto, C., Wisniewski, K. E., and Kida, E. (2004) Maturation of human tripeptidyl-peptidase I *in vitro*. *J. Biol. Chem.* **279,** 31058–31067
60. Saarela, J., Laine, M., Tikkanen, R., Oinonen, C., Jalanko, A., Rouvinen, J., and Peltonen, L. (1998) Activation and oligomerization of aspartylglucosaminidase. *J. Biol. Chem.* **273,** 25320–25328